Remote Sensing of Environment 114 (2010) 514–519

Contents lists available at ScienceDirect

Remote Sensing of Environment

journal homepage: www.elsevier.com/locate/rse

Improving the estimation of leaf area index by using remotely sensed NDVI with BRDF signatures

Kouiti Hasegawa [a,b,*], Hiroshi Matsuyama [a], Hayato Tsuzuki [c], Tatsuo Sweda [c]

[a] Department of Geography, Tokyo Metropolitan University, 1-1 Minami-Ohsawa, Hachioji, Tokyo 192-0397, Japan
[b] Department of Science, Komazawa University Senior High School, 1-17-12 Kami-Youga, Setagaya, Tokyo 158-8577, Japan
[c] Department of Agriculture, Ehime University, 3-5-7 Tarumi, Matsuyama, Ehime 790-8566, Japan

ARTICLE INFO

Article history:
Received 27 May 2009
Received in revised form 9 October 2009
Accepted 10 October 2009

ABSTRACT

A new vegetation index, the Normalized Hotspot-signature Vegetation Index (NHVI), is proposed for a better quantitative estimation of leaf area index (LAI) than with the remotely sensed normalized difference vegetation index (NDVI), especially in the boreal forest. To obtain this new index, the Hotspot–Dark-spot index (HDS) (Lacaze et al., 2002) was introduced. HDS is calculated by the difference between the strongest vector (hotspot) and the weakest vector (dark-spot) of bi-directional reflectance, a given tract of vegetation returns in the reflecting solar position, and the geometric structure of the vegetation canopy, which are poorly represented by NDVI alone. The validity of NHVI was statistically tested using two field data sets of multi-angular observations and LAI from the boreal forests of Canada; one set was our own observations, and the other was from the Boreal Ecosystem–Atmosphere Study (BOREAS). The range of linear correspondence of NHVI with LAI is much wider than that of NDVI alone, indicating significant representation of leaf biomass in the canopy geometry captured by HDS. With the technical innovation of multi-angular remote-sensing and kernel-driven models in the future, this index has the potential to provide a more accurate evaluation of regional and global LAIs.

© 2009 Published by Elsevier Inc.

1. Introduction

The leaf area index (LAI), defined as half the total developed area of leaves per unit ground horizontal surface area (Weiss et al., 2004), is an important biophysical parameter in ecophysiology, atmosphere–ecosystem interaction, and global climate change studies. Since energy, water, and trace gases are exchanged through the leaf surface, LAI is incorporated in many land-surface models, with its estimates derived from satellite-based vegetation indices such as the normalized difference vegetation index (NDVI).

$$\mathrm{NDVI} = \frac{(\mathrm{NIR}-\mathrm{RED})}{(\mathrm{NIR}+\mathrm{RED})} \tag{1}$$

Here, NIR is the reflectance of near-infrared bands, and RED is the reflectance of red bands.

Most spectral vegetation indices are based on the fact that the green leaves of vegetation absorb solar radiation in the red band. This signal is a function of fractional cover, leaf greenness, canopy depth, canopy lateral structure, and other conditions of vegetation; however, vegetation indices based on this signal have often successfully extracted the spread and distribution of vegetation (e.g., Carreiras et al., 2006; Lunetta et al., 2006).

In verifying satellite-derived LAIs against ground reference data obtained by the destructive method (hereafter, allometric LAI or *La*, see Section 3), there is a problem with saturation involving the non-linear relationship between LAI and NDVI as depicted in Fig. 1 (e.g., Baret & Guyot, 1991; Rautiainen, 2005; Hasegawa et al., 2006). Namely, the limited range of linearity makes proper estimation of LAI from NDVI difficult, especially when LAI exceeds 2.0. In Fig. 1, NDVI cannot distinguish LAI between 2.0 and 5.0. This saturation problem suggests that we must consider other elements, such as three-dimensional distribution of foliage, when estimating LAI in order to overcome this non-linearity. Thus, it is necessary to develop a new and more versatile vegetation index that is linearly correlated with LAI over a wider range.

One potential solution to this problem is multi-angular optical remote-sensing, which is capable of assessing three-dimensional vegetation structures that are not detectable by nadir observation alone (Chen et al., 2003; Gao et al., 2003; Brown de Colstoun & Walthall, 2006). Multi-angular observation can capture the uneven scattering of sunlight by vegetation, which is called the Bi-directional Reflectance Distribution Function (BRDF), so it should have the potential to evaluate LAI more accurately than simple nadir observation alone. Actually, some modeling communities have

* Corresponding author. Department of Geography, Tokyo Metropolitan University, 1-1 Minami-Ohsawa, Hachioji, Tokyo 192-0397, Japan. Tel.: +81 42 677 2603; fax: +81 42 677 2589.
E-mail address: k.hasegawa@amateras.geog.metro-u.ac.jp (K. Hasegawa).

0034-4257/$ – see front matter © 2009 Published by Elsevier Inc.
doi:10.1016/j.rse.2009.10.005

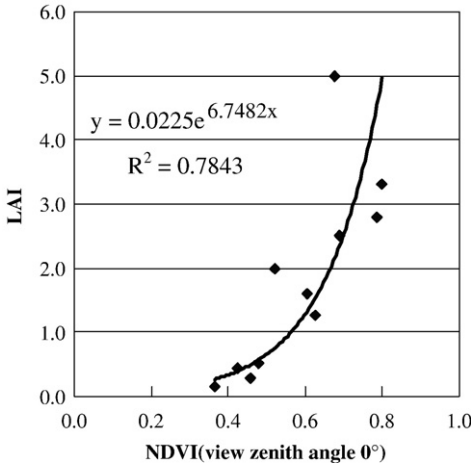

Fig. 1. Non-linear relationship between LAI and NDVI. (Data taken from Hasegawa et al., 2006, and BOREAS).

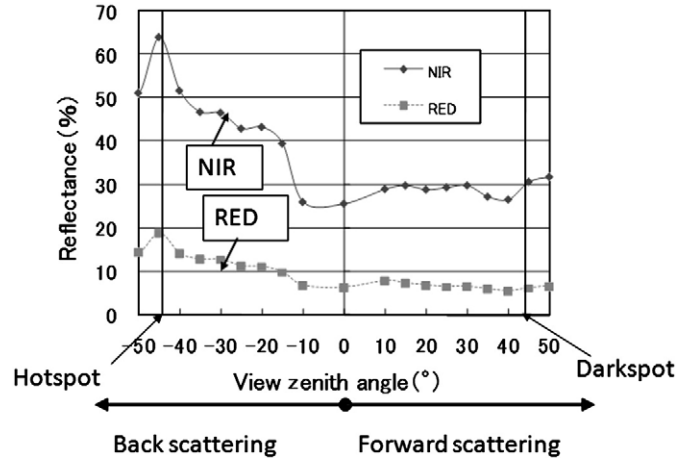

Fig. 2. Example of changes in the reflectance of red and near-infrared bands according to changes in the view zenith angle. Data were taken from Plot 4 of Table 1 (see Section 3.1).

proposed physical BRDF models that can truly invert LAI better than empirical vegetation indices (e.g., Bicheron & Leroy, 1999).

The physical modeling approach is a method used to estimate accurate LAI. However, the results differ from one model to another. In addition, the user must input many parameters to invert one vegetation parameter such as LAI. In contrast, the vegetation index is a useful tool for visual and objective vegetation monitoring. Therefore, this study focused on the development of a new vegetation index based on BRDF observations in the field with the use of the kernel model (Wanner et al., 1995).

Some multi-angular observation data are already available from sensors mounted on satellites (e.g., POLDER/ADEOS and ADEOS2, CHRIS/PROBA, and MISR/Terra). Although the spatial resolution of POLDER (6 km) is still too coarse to compare ground reference LAI data, those of CHRIS (17 m) and MISR (~275 m) are suitable (i.e., Heiskanen, 2006; Rautiainen et al., 2008). The viewing angles of these BRDF data are, however, too small to verify the new vegetation index that will be proposed in this study: CHRIS has five viewing angles, and MISR has nine. Also, the azimuth of these observations is rarely fixed by the orbit conditions.

It has been reported that the Hotspot–Dark-spot index (HDS), which is calculated from multi-angular optical remote-sensing data, adequately represented the geometric structures of vegetation (Lacaze et al., 2002, see Section 2). This study theoretically considers the relationship between HDS and LAI then proposes a new vegetation index, the Normalized Hotspot-signature Vegetation Index (NHVI). Finally, the NHVI validity was tested against LAI in terms of its linearity, using ground-based multi-angular optical observation of reflectances and simultaneous measurements of *La*.

2. Concept of new vegetation index

2.1. Hotspot, dark-spot, and HDS

Sunlight hitting the vegetation canopy is scattered unevenly as a result surface roughness, which is related to the canopy's shape and height. The reflectance is thus differentiated by view angle in multi-angular optical remote-sensing (Fig. 2). Also, the size and shape of the shadows of the vegetation structure vary, depending on solar position, canopy geometry, and sun-sensor configuration, causing variability in reflectance. As a typical characteristic of uneven scattering by vegetation, the strongest vectors of reflectance are expressed in the back-scattering direction, and the weakest are expressed in the forward-scattering direction (Fig. 2). Thus, in the following discussion, the azimuth of observation is relatively fixed as the direction of the Sun as seen from the observation point, and the term "multi-angular" refers to only the zenith angle of observation measured positively away from the Sun and negatively into the Sun. This observational plane is called the principal plane.

Fig. 2 plots the changes of reflectance with observational zenith angle for the red and near-infrared bands. The view zenith angle of 0° indicates a direction perpendicularly down from the observation point. As mentioned above, the side facing away from the Sun is referred to as the back-scattering region and is denoted here as negative, while the side facing into the Sun is referred to as the forward-scattering region and is denoted here as positive. The back-scattering region exhibits higher reflectance than the forward-scattering region since the former is basically sunlit while the latter is shaded. A peak in reflectance, known as the hotspot, occurs in the back-scattering region when the view zenith angle exactly matches the solar zenith angle in the principal plane. In Fig. 2, the hotspot is observed at 45°. Conversely, the weakest vector of reflectance appearing in the forward-scattering region is called the dark-spot.

Some previous studies (Lacaze et al., 2002; Chen et al., 2003; Gao et al., 2003) reported that the variability of reflectance in the principal plane is greatly modified by the amount of sunlit and shaded leaves in the canopy (i.e., under the same solar conditions where the leaves are more aggregated in clumps, the number of sunlit leaves decreases, while that of shaded leaves increases; consequently, the variability of reflectance increases).

The Hotspot–Dark-spot index (HDS; Lacaze et al., 2002) mentioned in Section 1 is defined as the difference in reflectance between the hotspot (ρHS) and the dark-spot (ρDS) relative to the reflectance at the dark-spot, and is calculated by Eq. (2).

$$\mathrm{HDS} = \frac{(\rho\mathrm{HS} - \rho\mathrm{DS})}{\rho\mathrm{DS}} \tag{2}$$

Obviously, a high HDS results from a strong contrast between the hotspot and dark-spot reflectances, which in turn is a manifestation of roughness in the canopy surface. This indicates that HDS is related to the canopy structure, such as the spatial distribution of foliage. When the reflectances of red and near-infrared bands are used for calculating HDS, HDS is both negatively and linearly correlated with the Clumping Index (Lacaze et al., 2002; see the next section), which is determined by the spatial distribution pattern of the leaves. One noteworthy fact is that the Clumping Index is a necessary parameter for estimating *La* based on ground-based measurements using the optical method (Chen and Cihlar, 1995a).

2.2. Direct and indirect measurements of LAI and their relationship with Clumping Index

Satellite-derived LAIs are usually verified against ground reference data, which is obtained either directly by destructive measurement of the leaves on the tree, or indirectly by optical instruments such as LAI-2000 (Li-COR Corporation) and hemispherical photography (Chen et al., 1997). In the indirect measurements, LAI is calculated from measured radiation transmittance (fraction gaps in the canopy) using inversion models based on the Lambert–Beer equation, which assumes a random spatial distribution of leaves (Welles & Norman, 1991). In this paper, LAI estimated in this way is referred to as the effective LAI and is denoted by *Le*. The advantage of this method is its speed and simplicity; thus, *Le* is used as ground reference data in the majority of remote-sensing studies for ecological modeling (Colombo et al., 2003; Houborg & Soegaard, 2004). However, this method usually underestimates LAI with significantly reduced accuracy compared with the direct method (Chen et al., 1997). This is because, in most forests (especially boreal forests), the canopy structure cannot be assumed to be homogeneous: leaves are grouped in shoots, shoots are distributed within branches, and branches are organized within tree crowns.

Hereafter, this paper refers to the direct method as the allometric method since it is based on the allometric relationship between the stem diameter and the quantity of leaves on the tree. Establishing this allometric relationship requires the destructive measurement of sample trees in which leaves are detached, weighed, converted to leaf area using another allometric relationship between leaf weight and area, and finally correlated to the stem diameter at breast height (DBH). By applying this leaf area–DBH relationship to the censused stem diameters of a given forest stand, the leaf area of each individual tree is obtained and then added together to obtain the total leaf area of the stand. This is the way *La* is estimated.

Usually, *Le* is smaller than *La*, so the Clumping Index (Ω) is introduced to solve this problem using the following equation (Chen & Cihlar, 1995a, b).

$$Le = La \times \Omega \tag{3}$$

We can calculate the Clumping Index based on the measurements of sunflecks by a light ceptometer in a forest on a fine day (Chen & Cihlar, 1995b). It has been reported that the product of *La* and the Clumping Index is almost equal to *Le* in boreal forests (Chen et al., 1997). Namely, the Clumping Index relates *La* and *Le*, the former being difficult to measure with optical instruments (e.g., LAI-2000) alone. This fact indicates that the Clumping Index represents the degree of errors as deduced from the assumption that the forest canopy has random foliage organization.

2.3. Proposal of the Normalized Hotspot-signature Vegetation Index (NHVI)

Vegetation indices such as NDVI are correlated with reductions in photosynthetically active radiation (PAR). The dependence of NDVI on LAI is based on the correspondence between the amount of leaves and the absorption of PAR (APAR) in the satellite-observed spectrum of solar reflection (Sellers et al., 1996; van den Hurk et al., 2003). The relationship between APAR and NDVI is linear (Sellers, 1985); hence, the relationship between the fraction of APAR (fAPAR) and LAI is described by Eq. (4).

$$\mathrm{fAPAR} = 1 - \exp(-k \cdot \mathrm{LAI}) \tag{4}$$

Eq. (4) and the LAI inversion model used in LAI-2000 (Welles & Norman, 1991) are based on the same concept that assumes a homogeneous canopy. In Eq. (4), k is a coefficient related to the spatial distribution and structure of foliage and leaves. Therefore, in coniferous forests, k changes in accordance with changes in the Clumping Index (i.e., the Clumping Index controls the relationship between LAI and fAPAR). Furthermore, the Clumping Index is negatively and linearly correlated with HDS (Lacaze et al., 2002), both of which control the relationship between LAI and NDVI.

From these theoretical considerations, it can be seen that HDS could be a useful index for estimating *La*. Here, we propose a new index called the Normalized Hotspot-signature Vegetation Index (NHVI) as the product of NDVI and HDS and defined by Eq. (5).

$$\mathrm{NHVI} = \mathrm{NDVI} \times \mathrm{HDS} \tag{5}$$

For estimating NHVI, NDVI is calculated from the reflectances of the near-infrared and red bands, observed in the nadir direction. HDS is calculated from Eq. (2) by applying the multi-angular optical remote-sensing data of the near-infrared band because BRDF of the near-infrared band demonstrated a smaller degree of seasonal change than did the red band in summer (Hasegawa et al., 2009). According to BRDF observations of a *larix leptolepis* forest from a tower in Japan (LAI 2.8; Hasegawa et al., 2009), HDS characteristically increased in the red band after the rainy season, indicating a possibility that BRDF of the red band was influenced by the physiological conditions of green leaves. Furthermore, reflectance values of the red band were very small, especially in the dark-spot, leading to a larger error for calculating HDS.

3. Validation

3.1. Data used for the analyses

The validity of NHVI was statistically tested using two field data sets of multi-angular observations and LAIs from the boreal forests of Canada; one was our own set of observations (Hasegawa et al., 2006), and the other was taken from the Boreal Ecosystem–Atmosphere Study (BOREAS) (http://www.daac.ornl.gov/; Chen et al., 1997; Gamon et al., 2004). For accurate validation, we used *La* rather than *Le*.

3.1.1. Our own field data

We conducted ground-based measurements of *La* along with observations from multi-angular optical remote-sensing in Canada in August 2004 (Hasegawa et al., 2006). We targeted only the vegetation in succession stages after a forest fire in northwestern Canada where LAI was less than 2.0 since BOREAS targeted mainly mature forests where LAI exceeded 2.0 (see next section). The study area is depicted in Fig. 3.

We conducted field surveys at four plots with different vegetation types in succession stages (i.e., grass with lichen, birch, spruce with lichen, and spruce and birch with lichen). In each plot, a quadrate of 1 m × 10 m was established. The area of the quadrate was determined considering the height and distribution of the major vegetation. In each plot, the quadrate was divided into blocks of 1 m × 1 m, where the total live weight of vegetation above the ground was measured.

The practical method for measuring the total live weight differed for each species. For the lower-layer vegetation (e.g., *Vaccinium vitis-idaea*, *Equisetum arvense*, and *Ledum groenlandicum*), which grew uniformly thick and occupied some portion of the ground surface, the area covered by each plant per unit area was inspected visually in every block (1 m^2). Combined with the measurement of the total live weight of each plant in this block, the live weight of each species per unit area (1 m^2) was estimated; then the total live weight of the lower-layer vegetation was then estimated as follows.

$$\begin{aligned}&\text{Total live weight of the lower-layer vegetation}\\&= \sum \frac{\text{area covered by each plant}}{\text{unit area}}\\&\quad \times (\text{live weight per unit area of each plant})\end{aligned} \tag{6}$$

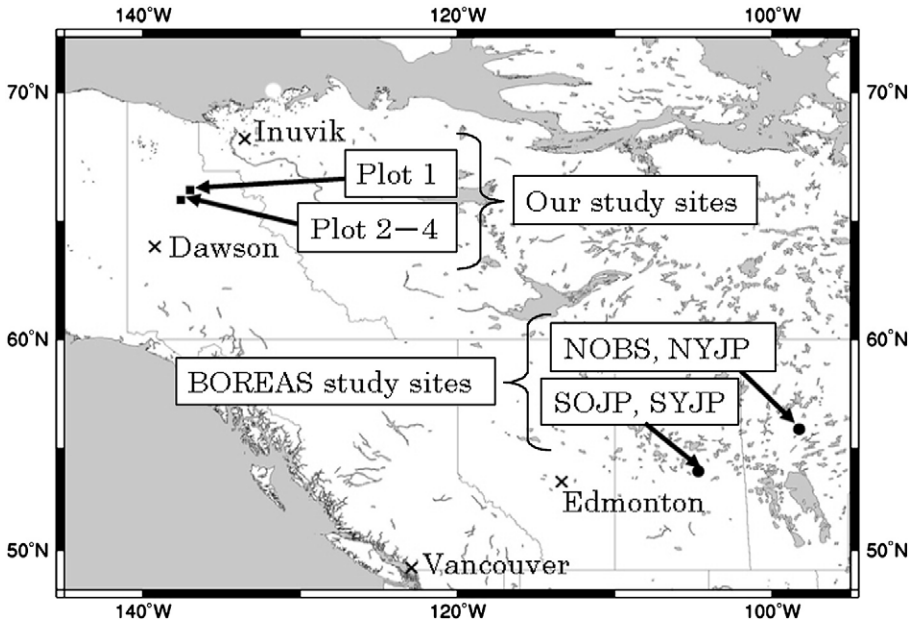

Fig. 3. Study area.

Two or more samples of grasses (e.g., fire weed) were taken to measure the weight of one leaf. After that, the total live weight was estimated by counting the number of grass plants. For stalk-like grasses such as sedge, the weight of one stalk was measured, then the total live weight of the stalk-like grasses was estimated by counting the number of stalks.

For the dominant species in the study area (*Picea glauca* or *mariana,* and *Betula glandulosa*), trunk diameters of the trees were measured to establish the regression equation with *La*. In each plot, five trees of several species with different trunk diameters were sampled. They were divided into trunks, branches, and leaves. After that, the total live weight was measured.

In all types of vegetation, 10% or more of the total live weight was taken as samples for each plant. The leaf surface areas of these samples were then measured by scanner with Scion Image Ver. 4.0.2 software (Scion Corporation). These samples were taken to Japan and were dried completely in the laboratory to calculate the ratio of biomass to leaf surface area, as well as to calculate the ratio of biomass to live weight. They were dried for at least two days at 85°. The *La* at each plot was calculated from these ratios and the total live weight of vegetation above the ground.

For BRDF measurements, an observer must change the view angle in a short time when the weather is fine. In this study, this condition was maintained by using a portable spectrum radiometer MS-720 (Eiko-Seiki Corp.), along with a portable 4 m-high tripod observation tower. MS-720 has a view angle of 45° and can observe reflectances from 350 to 1050 nm with 2 nm spectral resolution.

In each plot, the vegetation type of the square of the ground surface (32 m × 32 m) was assumed to be uniform and was verified by *in situ* visual inspection. The size of the square was determined considering the view angle of MS-720. The portable tower was located in the center of this square, where BRDF was measured from the top of the tower in order to minimize the influence of the observer's shadow.

BRDF was measured in the principal plane from 50° (forward-scattering direction) to −50° (back-scattering direction) by changing the observation angle in five-degree increments. Thirty minutes was required for the observation in each plot. The solar zenith angles at the time of the observations are presented in Table 1. When various vegetation indices were calculated, the reflectance of 443 nm (BLUE), 550 nm (GREEN), 670 nm (RED), and 864 nm (NIR) were selected for compatibility with the POLDER data in BOREAS (see next section). The precise information on the observations is presented in Table 1.

3.1.2. BOREAS data

In BOREAS, several kinds of optical remote-sensing data, including multi-angular optical remote-sensing, were observed from several platforms (e.g., an airplane, a tower, and a helicopter) in order to provide products needed for ecological planning and modeling. These data can be downloaded from the web site (http://www.daac.ornl.gov/; Gamon et al., 2004). Also, *La* was measured in BOREAS, which was described in detail by Chen et al. (1997).

Multi-angular optical remote-sensing data and *La* observed at four sites (northern old black spruce (NOBS), northern old jack pine (NOJP), southern old jack pine (SOJP), and southern young jack pine

Table 1
Precise information of each plot.

Plot number	Passage years after forest fire	Plot name	Allometric LAI	Observed date	Solar zenith angle (°)
Our study sites					
1	1–2	Grass with lichen	0.29	20th, Aug. 2004	45–50
2	10–20	Birch	0.52	20th, Aug. 2004	45–50
3	10–20	Spruce with lichen	1.26	19th, Aug. 2004	45–50
4	10–20	Spruce and birch with lichen	1.61	19th, Aug. 2004	40–45
BOREAS sites					
NYJP	25	Mature forest(young jack pine)	2.00	7th, Jun. 1994	33.1
SOJP	60–75	Old jack pine	2.50	21th, Jul. 1994	33–35
SYJP	11–16	Young jack pine	2.80	21th, Jul. 1994	35–38
NOBS	75–90	Mature forest (old black spruce)	5.00	7th, Jun. 1994	30.6

(SYJP)) were used. NOBS and NOJP are located in the BOREAS northern study area, while SOJP and SYJP are located in the BOREAS southern study area (Fig. 3). The main species in these sites are black spruce and jack pine.

The multi-angular optical remote-sensing data were obtained by POLDER mounted in a helicopter and on a tower (Gamon et al., 2004). These data consist of five bands: 443 nm (BLUE), 550 nm (GREEN), 670 nm (RED), 864 nm (NIR), and 910 nm (NIR). At NOBS and NYJP, BRDF was observed in the principal plane by changing the observation angle in one-degree increments. However, at SOJP and SYJP, BRDF was observed by changing the view azimuth angle and the view zenith angle randomly. We thoroughly inspected the data of the above web site and noted this fact.

3.2. Introduction of Ross–Li model to adjust for solar conditions

All BRDF data were acquired in the same season (Table 1); however, the solar zenith angles at the time of the BRDF observations were different. Therefore, it is necessary to adjust for solar conditions in order to compare these data. To this end, we used a semi-empirical BRDF model, the Ross–Li model (Wanner et al., 1995), to convert the BRDF data under the same solar conditions. This model is a major semi-empirical model to produce the MODerate resolution Imaging Spectroradiometer (MODIS) BRDF/Albedo products.

The semi-empirical BRDF model is based on linear combinations of "kernels."

$$\rho = f_{iso} + f_{geo}K_{geo} + f_{vol}K_{vol} \tag{7}$$

In Eq. (7), surface reflectance (ρ) is expressed as a combination of the function of component reflectance (f_x) and kernels (K_x). These mathematical functions depend on the solar zenith angle and the view zenith angle. Here, f_{iso} is equivalent to the reflectance acquired by nadir observation when the solar zenith angle is zero. The subscripts "geo" and "vol" refer to the physical bases for certain kernels in which "geometric" and "volume" scattering factors are identified.

In this study, K_{vol} and K_{geo} were calculated using the Ross Thick model and the Li-Sparse model from BRDF observational data (Wanner et al., 1995). Furthermore, the fitting algorithm in the GNUPLOT software (http://www.gnuplot.info/) was used to invert f_{iso}, f_{geo}, and f_{vol} from the reflectance and kernel datasets in each BRDF data.

Fig. 4 presents the results of the simulated multi-angular optical remote-sensing data at each plot for a solar zenith angle of 35°. From this figure, the highest reflectance is confirmed in the back-scattering region at the view zenith angle exactly matching the solar zenith angle, as previous studies have reported (Lacaze & Roujean, 2001; Peltoniemi et al., 2005). From Fig. 4, we defined the hotspot as 35°.

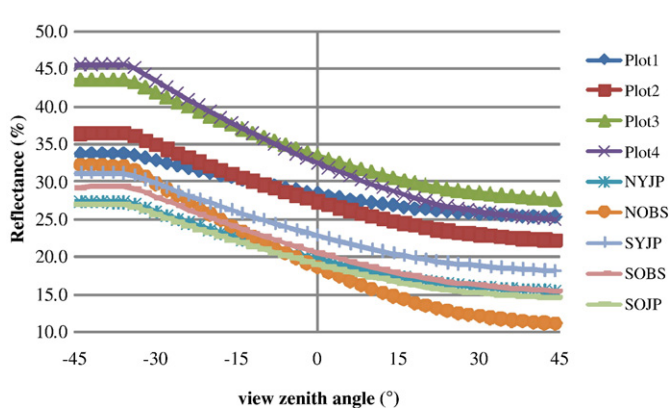

Fig. 4. Changes in the reflectance of the near-infrared band according to changes in the view zenith angle in the principal plane, simulated by a semi-empirical Ross–Li model with a solar zenith angle of 35°.

According to observational studies, the lowest vector of reflectance is not fixed because reflectance is uniformly low in this region (Lacaze & Roujean, 2001; Hasegawa et al., 2006). In this study, the dark-spot is defined as the same angle as the hotspot but in the forward-scattering direction, in order to extract the dark-spot objectively from multi-angular optical remote-sensing data. In Fig. 4, the dark-spot reflectance from this definition is not necessarily the lowest vector in this simulated data, located at greater than 35°. However, some BRDF observational studies (Lacaze & Roujean, 2001; Hasegawa et al., 2006) reported that when the view zenith angle became larger than the lowest vector direction, the reflectance became greater again (not simulated in this model (Fig. 4)). Therefore, we assume that the definition of dark-spot in this study is sufficient to confirm the potential of NHVI.

3.3. Comparison between NDVI/NHVI and allometric LAI (La)

Based on these definitions, hotspot and dark-spot reflectances were extracted from the datasets to obtain HDS for calculating NHVI. The scatter diagrams between NDVI/NHVI and *La* are depicted in Fig. 5 to highlight the efficacy of NHVI.

Fig. 5(a) illustrates the non-linear relationship between NDVI and *La*, which is approximated by an exponential function (Fig. 1). In contrast, the linear relationship between NHVI and *La* is confirmed in Fig. 5(b), as was predicted in Section 2. In Fig. 5(a) and (b), both correlation coefficients are statistically significant at the 1% level. Although NDVI cannot distinguish *La* exceeding 2.0 (Fig. 5a), NHVI can do so. Thus, we have demonstrated and suggested that NHVI is effective for estimating *La* in the boreal forests of Canada.

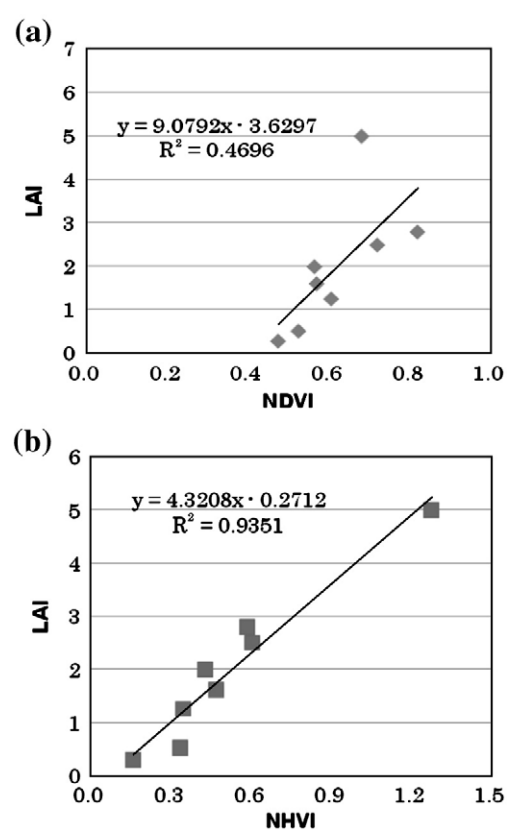

Fig. 5. Relationship between vegetation indices and *La*.

4. Conclusions

This study initially considered the relationship between the Hotspot–Dark-spot index (HDS) and allometric LAI (*La*). HDS is calculated from multi-angular optical remote-sensing data that express the geometric structure of vegetation. Based on this theoretical consideration, a new vegetation index, the Normalized Hotspot-signature Vegetation Index (NHVI), was proposed. NHVI is linearly correlated with *La* and is calculated from multi-angular optical remote-sensing data. The efficacy of NHVI was validated with our own field data collected in northwestern Canada in August 2004, along with BOREAS data.

We demonstrated that NHVI was superior to NDVI for estimating *La*, although this study was based on limited available data. From this result, we conclude that NHVI will be a useful tool for estimating *La* of boreal forests. The present study demonstrates the potential, but a more robust validation exercise is required. In the future, more BRDF data should be collected to thoroughly validate the efficacy of NHVI. Furthermore, the development of a kernel-driven BRDF model will enable simulating HDS and NHVI precisely from the multi-angular optical remote-sensing data of satellites, such as CHRIS/PROBA and MISR/Terra.

Acknowledgements

This study was supported in part by a Grant-in-Aid for Scientific Research (B) No. 19300310 (Principal Investigator: H. Matsuyama), Japan Society for the Promotion of Science. Constructive comments and recommendations by the editor and three anonymous reviewers for improving the original manuscript are greatly appreciated.

References

Baret, F., & Guyot, G. (1991). Potentials and limits of vegetation indices for LAI and APAR assessment. *Remote Sensing of Environment*, *35*, 161—173.

Bicheron, P., & Leroy, M. (1999). A method of biophysical parameter retrieval at global scale by inversion of a vegetation reflectance model. *Remote Sensing of Environment*, *67*, 251—266.

Brown de Colstoun, E. C., & Walthall, C. L. (2006). Improving global scale land cover classifications with multi-directional POLDER data and a decision tree classifier. *Remote Sensing of Environment*, *100*, 474—485.

Carreiras, J. M. B., Pereira, J. M. C., & Pereira, J. S. (2006). Estimation of tree canopy cover in evergreen oak woodlands using remote sensing. *Forest Ecology and Management*, *223*, 45—53.

Chen, J. M., & Cihlar, J. (1995). Quantifying the effect of canopy architecture on optical measurements of leaf area index using two gap size analysis methods. *IEEE Transactions on Geoscience and Remote Sensing*, *33*, 777—787.

Chen, J. M., & Cihlar, J. (1995). Plant canopy gap-size analysis theory for improving optical measurements of leaf area index. *Applied Optics*, *34*, 6211—6222.

Chen, J. M., Rich, P. M., Gower, S. T., Norman, J. M., & Plummer, S. (1997). Leaf area index of boreal forests: Theory, techniques, and measurements. *Journal of Geophysical Research*, *102*, 29429—29443.

Chen, J. M., Liu, J., Leblanc, S. G., Lacaze, R., & Roujean, J. -L. (2003). Multi-angular optical remote sensing for assessing vegetation structure and carbon absorption. *Remote Sensing of Environment*, *84*, 516—525.

Colombo, R., Bellingeri, D., Fasolini, D., & Marino, C. M. (2003). Retrieval of leaf area index in different vegetation types using high resolution satellite data. *Remote Sensing of Environment*, *86*, 120—131.

Gamon, J. A., Huemmrich, K. F., Peddle, D. R., Chen, J., Fuentes, D., Hall, F. G., Kimball, J. S., Goetz, S., Gu, J., McDonald, K. C., Miller, J. R., Moghaddam, M., Rahman, A. F., Roujean, J. -L., Smith, E. A., Walthall, C. L., Zarco-Tejada, P., Hu, B., Fernandes, R., & Cihlar, J. (2004). Remote sensing in BOREAS: Lessons learned. *Remote Sensing of Environment*, *89*, 139—162.

Gao, F., Schaaf, C. B., Strahler, A. H., Jin, Y., & Li, X. (2003). Detecting vegetation structure using a kernel-based BRDF model. *Remote Sensing of Environment*, *86*, 198—205.

Hasegawa, K., Matsuyama, H., Tsuzuki, H., & Sweda, T. (2006). The effect of bi-directional reflectance distribution function on the estimation of vegetation indices and leaf area index (LAI) — A case study of the vegetation in succession stages after forest fire in Northwestern Canada. *Journal of the Remote Sensing Society of Japan*, *26*, 186—201 (in Japanese with English abstract).

Hasegawa, K., Izumi, T., Matsuyama, H., Kajiwara, K., & Honda, Y. (2009). Relationship between the bidirectional reflectance distribution function in *Larix leptolepis* and its phenology. *Proceedings of the General Meeting of the Japanese Forest Society, March, Kyoto, MaPa1-21* in Japanese.

Heiskanen, J. (2006). Tree cover and height estimation in the Fennoscandian tundra–taiga transition zone using multiangular MISR data. *Remote Sensing of Environment*, *103*, 97—114.

Houborg, R. M., & Soegaard, H. (2004). Regional simulation of ecosystem CO_2 and water vapor exchange for agricultural land using NOAA/AVHRR and Terra MODIS satellite data. Application to Zealand, Denmark. *Remote Sensing of Environment*, *93*, 150—167.

Lacaze, R., & Roujean, J. (2001). G-function and HOT Spot (GHOST) reflectance model application to multi-scale airborne POLDER measurements. *Remote Sensing of Environment*, *67*, 67—80.

Lacaze, R., Chen, J. M., Roujean, J. -L., & Leblanc, S. G. (2002). Retrieval of vegetation clumping index using hot spot signatures measured by POLDER instrument. *Remote Sensing of Environment*, *79*, 84—95.

Lunetta, R. S., Knight, J. F., Ediriwickrema, J., Lyon, J. G., & Worthy, L. D. (2006). Land-cover change detection using multi-temporal MODIS NDVI data. *Remote Sensing of Environment*, *105*, 142—154.

Peltoniemi, J. I., Kaasalainen, S., Naranen, J., Rautiainen, M., Stenberg, P., Smolander, H., Smolander, S., & Voipio, P. (2005). BRDF measurement of understory vegetation in pine forests: Dwarf shrubs, lichen, and moss. *Remote Sensing of Environment*, *94*, 343—354.

Rautiainen, M. (2005). Retrieval of leaf area index for coniferous forest by inverting a forest reflectance model. *Remote Sensing of Environment*, *99*, 295—303.

Rautiainen, M., Lang, M., Mottus, M., Kuusk, A., Nilson, T., Kuusk, J., & Lukk, T. (2008). Multi-angular reflectance properties of a hemiboreal forest: An analysis using CHRIS PROBA data. *Remote Sensing of Environment*, *112*, 2627—2642.

Sellers, P. J. (1985). Canopy reflectance, photosynthesis and transpiration. *International Journal of Remote Sensing*, *6*, 1335—1372.

Sellers, P. J., Los, S. O., Tucker, C. J., Justice, C. O., Dazlich, D. A., Collatz, G. J., & Randall, D. A. (1996). A revised land surface parameterization (SiB2) for atmospheric GCMs. *Part II: The generation of global fields of terrestrial biophysical parameters from satellite data. Journal of Climate*, *9*, 706—737.

van den Hurk, B. J. J. M., Viterbo, P., & Los, S. O. (2003). Impact of leaf area index seasonality on the annual land surface evaporation in a global circulation model. *Journal of Geophysical Research*, *108*(D6), 4191. doi:10.1029/2002JD002846.

Wanner, W., Li, X., & Strahler, A. H. (1995). On the derivation of kernels for kernel-driven models of bidirectional reflectance. *Journal of Geophysical Research*, *100*, 21077—21089.

Weiss, M., Baret, F., Smith, G. J., Jonckheere, I., & Coppin, P. (2004). Review of methods for *in situ* leaf area index (LAI) determination Part II. Estimation of LAI, errors and sampling. *Agricultural and Forest Meteorology*, *121*, 37—53.

Welles, J. M., & Norman, J. M. (1991). Instrument for indirect measurement of canopy architecture. *Agronomy Journal*, *83*, 818—825.